8-13-2010

Transition Metal Dopants Essential for Producing Ferromagnetism in Metal Oxide Nanoparticles

Lydia M. Johnson
Boise State University

Aaron Thurber
Boise State University

Joshua Anghel
Boise State University

Maryam Sabetian
Boise State University

Mark H. Engelhard
Pacific Northwest National Laboratory

See next page for additional authors

Transition Metal Dopants Essential for Producing Ferromagnetism in Metal Oxide Nanoparticles

Lydia M. Johnson
Boise State University

Mark H. Engelhard
Pacific Northwest National Laboratory

Aaron Thurber
Boise State University

Dmitri A. Tenne
Boise State University

Josh Anghel
Boise State University

Charles B. Hanna
Boise State University

Maryam Sabetian
Boise State University

Alex Punnoose
Boise State University

Abstract

Recent claims that ferromagnetism can be produced in nanoparticles of metal oxides without the presence of transition metal dopants have been challenged in this work by investigating 62 high quality well-characterized nanoparticle samples of both undoped and Fe doped (0-10% Fe) ZnO. The undoped ZnO nanoparticles showed zero or negligible magnetization, without any dependence on the nanoparticle size. However, chemically synthesized $Zn_{1-x}Fe_xO$ nanoparticles showed clear ferromagnetism, varying systematically with Fe concentration. Furthermore, the magnetic properties of $Zn_{1-x}Fe_xO$ nanoparticles showed strong dependence on the reaction media used to prepare the samples. The zeta potentials of the $Zn_{1-x}Fe_xO$ nanoparticles prepared using different reaction media were significantly different, indicating strong differences in the surface structure. Electron paramagnetic resonance studies indicate that the difference in the ferromagnetic properties of $Zn_{1-x}Fe_xO$ nanoparticles with different surface structures originates from differences in the fraction of the doped Fe ions that participate in ferromagnetic resonance.

Introduction

Development of new magnetic materials by doping semiconducting metal oxides with transition metal (TM) ions has been reported extensively since the prediction of room temperature ferromagnetism (RTFM) in these oxides[1-3]. However, some recent reports claimed that RTFM can be produced in metal oxides without any TM dopants, if prepared in nanoparticle (NP)[4-7] or thin-film forms[8-11]. For example, based on experiments using an extensive set of metal oxides including ZnO, Sundaresan et al.[4] have reported that undoped NP (size 7-30nm) samples of these oxides displayed ferromagnetism at room temperature while their bulk counterparts were diamagnetic. They argued that the ferromagnetism resulted from the exchange interactions between localized electron spin moments produced by the oxygen vacancies on the NP surface. Further, Garcia et al.[6] reported that by modifying the surface through the capping of 10 nm NPs with three different organic molecules, they could achieve variations in the magnetic properties of undoped ZnO NP. A combined theoretical and experimental study by Fernandez et al. [11] argued that RTFM is possible in undoped ceria. Similar magnetism has also been reported in other non-magnets such as gold, silicon, and graphite [12-15]. In order to determine the likelihood of these claims, we prepared an extensive series of NP samples of zinc oxide with well defined sizes in the 4 to 20 nm range with (38 samples) and without (24 samples) Fe dopant, and investigated these samples thoroughly using a wide range of experimental techniques. The samples were synthesized by a chemical route that allows systematic variation of size, Fe dopant concentration, and reaction solvent to control the surface structure. If the magnetism is a result of active spin

moments on the particle surface, the sample magnetization must increase systematically with decreasing particle size. Our studies did not show any systematic dependence of the saturation magnetization with NP size, rather, appreciable RTFM was observed in the NP samples only if they contained Fe dopants. The observed magnetization varies strongly with Fe doping concentration and the surface structure. Interestingly, none of the undoped NP samples showed any appreciable ferromagnetism. These results suggest that the ferromagnetism observed in undoped metal oxide NPs is likely of impurity origin. While intentional alteration of NP surface structure can affect the strength of observed magnetization, TM dopants are necessary for the origination of appreciable RTFM.

Experimental Details

Zinc oxide NPs were prepared using similar chemical hydrolysis methods[16], one in diethylene glycol and the other in denatured ethanol solutions, hereafter referred to as ZnO-I and ZnO-II respectively. The samples were prepared from the same zinc acetate dihydrate precursor. Since two different solvents were used, the NPs should have different surface structure/groups depending on whether the particles are made by method I or method II. By varying the hydrolysis ratio (water : zinc acetate), ZnO-I samples were prepared in the 4-20 nm range, and by varying the reaction time, ZnO-II samples were prepared in the 4-9 nm range. In order to study the effect of TM dopant on the magnetic properties, samples were also prepared with iron ions doped using co-precipitation employing zinc and iron acetates in the hydrolysis process. The dopant concentration *x* is given by the molar ratio of [Fe]/([Fe]+[Zn]). Samples were characterized and investigated in detail using x-ray diffraction (XRD), magnetometry, transmission electron microscopy (TEM), Zeta potential measurements, electron paramagnetic resonance spectroscopy (EPR), and x-ray photoelectron spectroscopy (XPS).

X-ray diffraction (XRD) spectra were recorded at room temperature on a Philips X'Pert x-ray diffractometer with a Cu K_α source (λ = 1.5418 Å) in Bragg-Brentano geometry. The loose powder samples were leveled in the sample holder to ensure a smooth surface and mounted on a fixed horizontal sample plane. Data analyses were carried out using profile fits of selected individual XRD peaks.

Zeta potentials of the powdered samples of undoped ZnO NPs and $Zn_{1-x}Fe_xO$ NPs were measured in nanopure water as a function of pH with a Malvern Zetasizer NanoZS. The temperature was equilibrated to 25°C, and the pH was varied in the 6 to 12 range using 1.0 N HCl and 1.0 N NaOH prior to collecting the data. At least 8 data collections per run were performed on three separate aliquots of the ZnO suspension for each sample.

High-resolution TEM analysis was carried out on a JEOL JEM-2100HR microscope with a specified point-to-point resolution of 0.23 nm. The operating voltage of the microscope was 200 kV. Image processing was carried out using the Digital Micrograph software from Gatan (Pleasant, California, USA).

For XPS measurements, the Fe doped ZnO powders were mounted onto the XPS sample holder by pressing onto double sided Nichiban tape inside a 3 mm diameter Moly finger mask. XPS spectra were recorded using a Physical Electronics Quantum 2000 Scanning ESCA Microprobe available at the Pacific Northwest National Laboratory. This system uses a focused monochromatic Al K_α x-ray (1486.7 eV) source and a spherical section analyzer. The instrument has a 16 element multichannel detector. The X-ray beam used was a 100 W, 100 μm diameter beam that was rastered over a 1.3 mm by 0.2 mm rectangle on the sample. The X-ray beam is incident normal to the sample and the photoelectron detector was at 45° off-normal. The high energy resolution photoemission spectra were collected using a pass energy of 46.95 eV. For the $Ag3d_{5/2}$ line, these conditions produced FWHM of better than 0.98 eV. The binding energy (BE) scale is calibrated using the $Cu2p_{3/2}$ feature at 932.62 ± 0.05 eV and Au 4f at 83.96 ± 0.05 eV for known standards. The samples experienced variable degrees of charging. Low energy electrons at ~1 eV, 20μA and low energy Ar^+ ions were used to minimize this charging. The spectra shown here were charge referenced using the C 1s line at 284.8 eV.

Magnetic measurements were carried out at room temperature using a LakeShore model 7404 vibrating sample magnetometer by tightly packing powder samples placed in a clear plastic drinking straw. The magnetization data was recorded as a function of applied magnetic field up to ±1 T. The data reported here were corrected for the background signal from the sample holder (clear plastic drinking straw) with diamagnetic susceptibility $\chi = -4.1 \times 10^{-8}$ emu/Oe.

Electron paramagnetic resonance (EPR) measurements of the powder samples were performed. Small amounts (~ 40 mg) of each powder were placed in quartz tubes and inserted into the microwave cavity of a Bruker ELEXSYS E-500 X-band spectrometer. Sample temperature was maintained by a liquid nitrogen coldfinger flask. The data shown here were taken at 77 K using a modulation amplitude of 1 G.

Results and discussion

XRD was employed to investigate the structural properties and crystallite size, and to rule out the presence of any unwanted impurity phases. The representative XRD patterns shown in Figure 1a display only the wurtzite ZnO phase with no indication of other phases even in the sample with the highest Fe concentration of 10%. Since the XRD system used in this work has a detection ability of chemical phases with more than 1.5% (determined from XRD measurements of a physical mixture of ZnO and α-Fe_2O_3), this clearly rules out the presence of any crystalline iron oxides or other binary oxides. The XRD peak positions of both ZnO-I and ZnO-II showed gradual changes with Fe doping, revealing interesting variations in the lattice parameters *a* and *c* and lattice volume V, determined using suitable pairs of (100), (102), (110) and (103) peaks, as shown in Figure 1b. This provides evidence for increasing incorporation of Fe ions in ZnO crystallites since the ZnO lattice volume initially increases due to Fe doping up to 5%. This can be understood qualitatively considering the sizes and charges of the ions and their local coordinations when Fe ions substitute for Zn^{2+} ions. This might also require rearrangement of neighboring oxygen and/or Zn^{2+} ions for charge neutrality. The relatively mild, but opposite changes in the lattice volume for >5% doping indicates additional incorporation of dopant ions in interstitial sites as has been reported in some host systems causing somewhat similar structural changes in the lattice parameters [17, 18]. Analysis of lattice parameters for the undoped NPs of both ZnO-I and ZnO-II samples showed a gradual increase in the unit cell volume V with decreasing particle size L as shown in Figure 1c. A similar increase in V with decreasing L has been observed in other oxide NP systems also due to their large surface to volume ratio [19].

Average crystallite size L of the undoped ZnO NPs and the doped $Zn_{1-x}Fe_xO$ NPs were calculated using the width of the (102) peak and the Scherrer relation, $L = \frac{0.9\lambda}{B\cos\theta}$ (where θ is the peak position, λ is the x-ray wavelength and peak width $B = (B_m^2 - B_s^2)^{1/2}$ was estimated using the measured peak width B_m and the instrumental width B_s). The crystallite sizes of all the $Zn_{1-x}Fe_xO$-I and $Zn_{1-x}Fe_xO$-II NP were 6.8±0.6nm and 6.9±0.2nm respectively. Average L for undoped ZnO-I samples were ~ 4, 8, 13 and 20 nm and ZnO-II NP were ~ 3.9, 4.4, 5.6, 6.9, 7.8, 8.3 and 9.0 nm. TEM images (Figure 2) of Fe doped $Zn_{1-x}Fe_xO$ NPs and pure ZnO NPs smaller than 10 nm showed nearly spherical particles. For ZnO NPs larger than 10 nm, the particles become somewhat elongated. Particle size distribution analysis of the samples conducted using TEM images confirmed that the particle size variations of all the samples employed here are within approximately ±4nm (see Figure 2).

Unlike bulk materials, NPs have large surface to volume ratio and the NP surface consists of uncompensated charged ions. ZnO-I and ZnO-II NP were synthesized in two different solution media, namely DEG and ethanol respectively, and therefore their surface structure and charge are expected to be different. To obtain insight into their surface structure and charge, zeta potentials of the powdered samples of undoped ZnO NPs and Fe doped $Zn_{1-x}Fe_xO$ NPs suspended in nanopure water were measured as a function of pH. Zeta potential at pH of ~ 7.5 showed differing surface charge for samples prepared in DEG and ethanol, with ZnO-I samples averaging to ~ +40±5.0 mV and ZnO-II samples giving less than half that at ~ +15 ±12.0 mV. Zeta potentials of ZnO-I and ZnO-II NPs as a function of pH for different crystallite sizes are shown in Figure 3. Zeta potentials of all the $Zn_{1-x}Fe_xO$-I NPs were similar at +33±1.4 mV suggesting that the Fe doping did not modify the surface charge significantly. This is true for the $Zn_{1-x}Fe_xO$-II set also, although with a lower zeta potential of +18±2.1mV. Thus, these measurements clearly demonstrate that the zeta potentials and therefore the surface structure of the NP samples prepared in DEG medium (set I) and ethanol medium (set II) are significantly different.

XPS measurements were employed to investigate the possible presence of any iron oxides in the $Zn_{1-x}Fe_xO$ crystallites. The Fe $3p_{1/2}$ XPS spectral region of $Zn_{1-x}Fe_xO$-II NPs with different x is shown in Figure 4. The core level Fe $3p_{1/2}$ peak was observed at ~54.7 eV and 55.2 eV for $Zn_{1-x}Fe_xO$-I and $Zn_{1-x}Fe_xO$-II NPs respectively. These binding energy values are clearly different from the binding energies of Fe $3p_{1/2}$ peak expected for most common iron oxides such as magnetite (53.9 eV), hematite (55.7 eV) and maghemite (55.7 eV) [20, 21]. This rules out the presence of these common iron oxides in $Zn_{1-x}Fe_xO$ samples and also clearly demonstrates the difference in the

atomic environment surrounding the incorporated Fe ions in $Zn_{1-x}Fe_xO$ from that of these oxides. Thus, the XPS data clearly suggest that the Fe peaks observed from the $Zn_{1-x}Fe_xO$ samples are not arising from any maghemite, hematite or magnetite inclusions in the samples.

Room temperature magnetization M vs. magnetic field H measurements were carried out on all the samples. The resulting hysteresis loops were analyzed to determine the saturation magnetization M_s, remanence M_r and coercivity H_c of these samples. A few representative hysteresis loops of doped and undoped ZnO-I and ZnO-II are shown in Figure 5. The undoped ZnO-I and ZnO-II NP samples showed closed or very weak hysteresis loops, with M_s in the 0-1memu/g, M_r in the 0-0.05memu/g and H_c in the 0-300G range. The hysteresis loop parameters showed that varying size of the ZnO NP samples prepared using both methods (ZnO-I and ZnO-II) in the 4 to 20nm range did not result in systematic changes in M_s (Figure 6a), H_c (Figure 6b), or M_r. If the magnetism is arising from the surface of undoped NPs as other reports have claimed[4-7], the observed weak magnetism should have varied systematically with particle size. The random variation of the magnetization of the undoped ZnO with decreasing particle size therefore indicates that the ferromagnetism is most likely arising from weak impurities present in these samples that were so low in concentration to escape detection in the characterization studies. The extremely large surface of NPs is more likely to adsorb impurity atoms/ions compared to that of their bulk counterparts. Note that ferromagnetism has been reported in metal oxides doped with even < 0.5% of TM ions[18]. Our NP samples of pure undoped ZnO were prepared in the 4 to 20nm range, which covers the sizes used by all the studies [4-7] that reported ferromagnetism in undoped ZnO NPs, and measurements were conducted on 24 independently synthesized ZnO NP samples to ensure that our results are statistically significant.

Doping ZnO NPs with Fe had dramatic effects on the magnetic properties, showing a systematic increase in M_s with increasing Fe content, as shown in Figure 6c. This result clearly suggests that TM dopants are essential to produce ferromagnetism in ZnO. The $Zn_{1-x}Fe_xO$-II samples showed much stronger magnetization compared to $Zn_{1-x}Fe_xO$-I. For example, for 10% Fe concentration, the $Zn_{1-x}Fe_xO$-II samples displayed 20 times stronger M_s than $Zn_{1-x}Fe_xO$-I. Since these two sets of samples were prepared following a similar procedure, but in different reaction media, the only difference expected is in their surface structure as evidenced from the significantly different zeta potentials. Thus, it can be concluded that the difference in the surface structure of $Zn_{1-x}Fe_xO$-I and $Zn_{1-x}Fe_xO$-II is responsible for the observed difference in ferromagnetism between the two sets.

One might argue that the observed magnetism might be due to superparamagnetism resulting from isolated DMS NP or possible nanoscale non-DMS FM inclusions. However, the magnetization data shown in Figure 5b (inset) clearly displays an open loop, and all Fe doped samples consistently displayed coercivity in the 30-240G range. Presence of clear coercivity rules out the possibility of superparamagnetism and supports a ferromagnetic origin. If the superparamagnet is below its blocking temperature, ferromagnetic-like behavior with open hysteresis loop is possible. However, this will require a blocking temperature well above room temperature. Further, regarding the possibility of some non-DMS ferromagnetic/superparamagnetic impurity phase being present in the sample, our detailed characterization studies using XRD and XPS have clearly ruled out the possible presence of metallic Fe, its magnetic oxides or Fe-Zn binary oxides. Samples doped with Fe% as high as 10% also showed no impurity phases. Further, random presence of such impurities is unlikely to produce a systematic increase in magnetization with increasing Fe%.

EPR spectroscopy is a very powerful and sensitive experiment to determine the oxidation state of Fe ions and their interactions. EPR spectra collected from $Zn_{1-x}Fe_xO$-I NPs at 77K, shown in Figure 7, consist of a set of sharp lines in the 1500 G to 3300 G range, and an additional broad signal centered around g ~ 2.05, with a linewidth of 2142 G. The sharp lines are attributable to several magnetically inequivalent high-spin Fe^{3+} ions (S = 5/2), characterized by different spin-Hamiltonian parameters, based on detailed studies reported on Fe doped ZnO single crystals and powders in the literature [22-24]. The broad signal, suggestive of ferromagnetically coupled Fe ions, is expected in semiconductors when doped with TMs if adequate charge carriers or oxygen vacancies are present[2, 3, 25]. . Another possible origin for the broad signal is inclusions of non-DMS FM NP such as iron oxides that might behave as superparamagnets. However, the detailed characterization data discussed earlier indicates that presence of such phases is an unlikely possibility. Interestingly, the EPR spectra (Figure 7) recorded from $Zn_{1-x}Fe_xO$-II NPs did not show any of the sharp lines, and only the broad signal attributed to Fe ions in ferromagnetic resonance was observed. Since the only difference expected between $Zn_{1-x}Fe_xO$-I and $Zn_{1-x}Fe_xO$-II NPs is in their surface structure, this result offers evidence that the observed EPR signals are primarily from Fe ions incorporated on the surface

region of the ZnO crystallites. In $Zn_{1-x}Fe_xO$-II NPs, there may be adequate oxygen vacancies/carriers on the NP surface to establish ferromagnetic coupling between all the doped ions, thus producing only a single but stronger signal due to the ferromagnetic component, and stronger magnetization[26]. The EPR data collected therefore confirms that the surface structure of NPs plays a crucial role in the observed ferromagnetic behavior, and explaining why the $Zn_{1-x}Fe_xO$-II NPs are stronger ferromagnets than the $Zn_{1-x}Fe_xO$-I NPs.

Conclusion

In summary, the detailed experimental studies described above on well characterized samples of undoped and Fe doped ZnO NPs clearly demonstrate that while surface structure can influence the strength of observed magnetism, TM dopants are necessary to produce an appreciable ferromagnetism in ZnO NPs. The NP samples of pure undoped ZnO prepared in the 4 to 20nm range, which covers the sizes used in all the recent reports claiming ferromagnetism in undoped ZnO NPs, showed zero or negligible magnetism. The observed magnetization did not show a systematic increase with decreasing particle size (ie, increasing particle surface) of the ZnO NPs, thus demonstrating that defects present increasingly in NPs because of their large surface to volume ratio are not solely responsible for the observed ferromagnetism in undoped metal oxide NPs. On the other hand, similar ZnO NPs synthesized with a TM ion (Fe) doped intentionally using identical synthesis procedures showed ferromagnetism and their magnetization varied systematically with Fe% (0 to 10% range), thus underlining that TM dopants are essential for ferromagnetism in metal oxides. These results make one wonder if the magnetism observed in undoped oxide NPs (especially those prepared using similar synthesis methods) is truly intrinsic or if it results from weak impurity/TM inclusions that are too low to be detected in most characterization tools. This work also compared the effect of different surface structures on the magnetism of Fe doped ZnO NPs and indeed observed significant differences in M_s (up to 20 times) suggesting that the NP surface structure plays a key role in the modification of magnetic properties. This work thus provides a new method to improve the ferromagnetic properties of TM doped metal oxides through careful tailoring of the surface structure.

Acknowledgements

This work was supported in part by the NSF-CAREER program (DMR-0449639), DoE-EPSCoR program (DE-FG02-04ER46142), ARO Grant No. W911NF-09-1-0051, NSF-MRI awards (#0722699 and #0521315), and NSF-RUI (DMR-0840227). A portion of the research described in this paper was performed in the Environmental Molecular Sciences Laboratory, a national scientific user facility sponsored by the Department of Energy's Office of Biological and Environmental Research and located at Pacific Northwest National Laboratory.

Figure captions

Figure 1. Panel (a) shows sample XRD patterns of ZnO-I, ZnO-II, $Zn_{1-x}Fe_xO$-I and $Zn_{1-x}Fe_xO$-II NPs. Drop lines indicate the expected XRD peak positions and relative intensities. Also shown is the variation in unit cell volume V for (b) $Zn_{1-x}Fe_xO$-I and $Zn_{1-x}Fe_xO$-II NPs as a function of *x* and (c) ZnO-I and ZnO-II NPs as a function of L.

Figure 2. Top panels show size distribution plots of NPs with average size of 4nm and 8nm for (a) ZnO-I and (b) ZnO-II. The middle row of panels show TEM images of ZnO-I NPs of (c) 4nm and (d) 20 nm size and (e) $Zn_{1-x}Fe_xO$-I for $x = 0.05$. The bottom row of panels show TEM images of ZnO-II NPs of (f) 4nm and (g) 9 nm size and (h) $Zn_{1-x}Fe_xO$-II for $x = 0.05$.

Figure 3. Zeta potentials of 5 mM NP concentration in nanopure water as a function of pH for (a) 4 and 20nm sized ZnO-I and $Zn_{1-x}Fe_xO$-I with $x = 0.10$ and (b) 4 and 9nm sized ZnO-II and $Zn_{1-x}Fe_xO$-II with $x = 0.10$.

Figure 4. Plot showing the Fe $3p_{1/2}$ XPS spectral region of $Zn_{1-x}Fe_xO$-II NPs with different *x* indicated. The vertical line is positioned at 55.2 eV.

Figure 5. Room temperature M vs. H measurements on powders of selected (a) ZnO-I and ZnO-II samples and (b)$Zn_{1-x}Fe_xO$-I and $Zn_{1-x}Fe_xO$-II NP samples. Insets show the low field regions of the same data.

Figure 6 (a) Variation of the saturation magnetization M_s vs. particle size L plotted for both ZnO-I and ZnO-II NPs, (b) Variation of the coercivity H_c vs. particle size L plotted for both ZnO-I and ZnO-II NPs, and (c) M_s vs. Fe concentration of $Zn_{1-x}Fe_xO$-I and $Zn_{1-x}Fe_xO$-II NPs. Inset shows expansion of the same $Zn_{1-x}Fe_xO$-I data.

Figure 7. 77K EPR spectra of $Zn_{1-x}Fe_xO$-I and $Zn_{1-x}Fe_xO$-II NPs with varying Fe concentration as indicated. The M_s values, obtained from magnetometry measurements of the same samples, are also included.

Figures

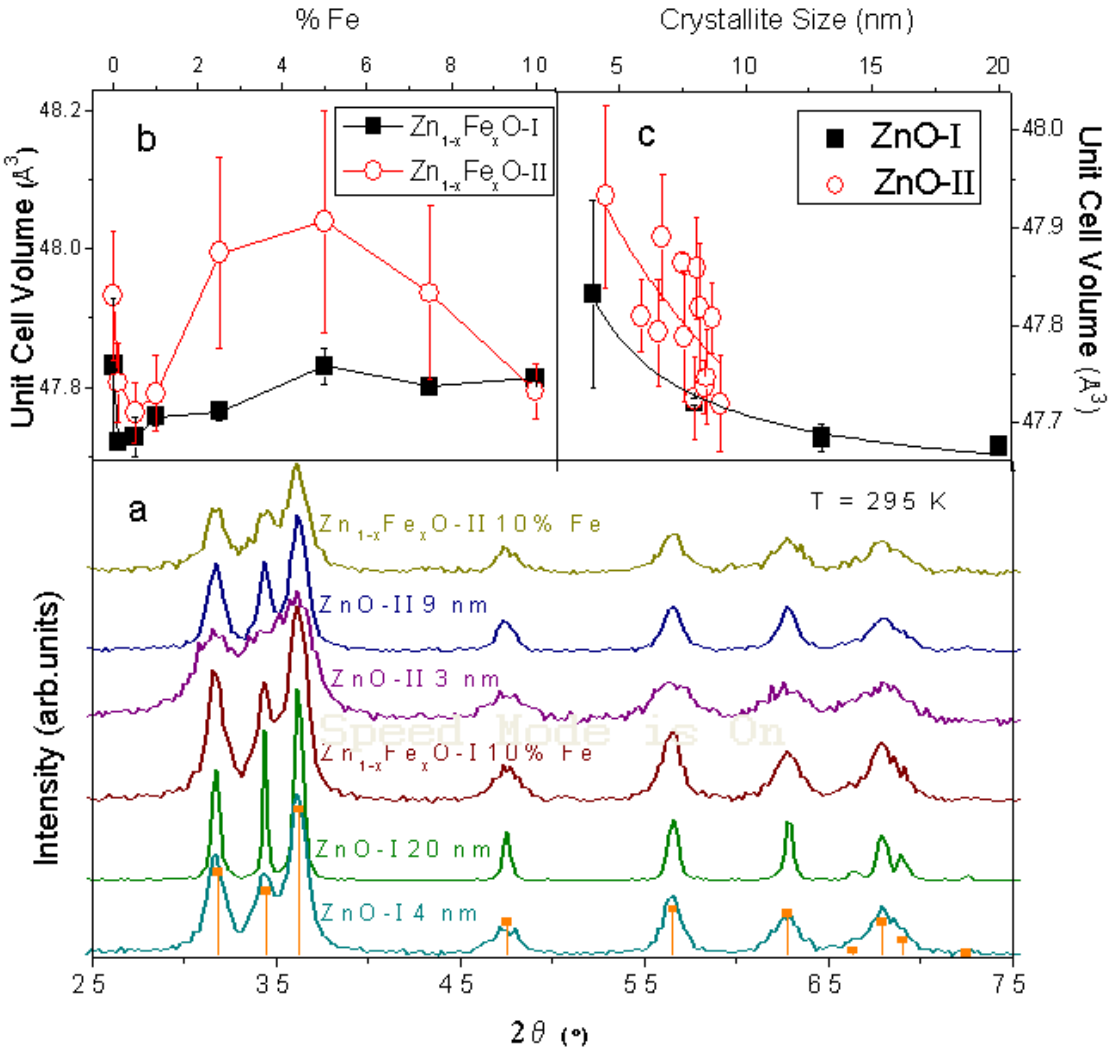

Figure 1, L. Johnson et al (color online)

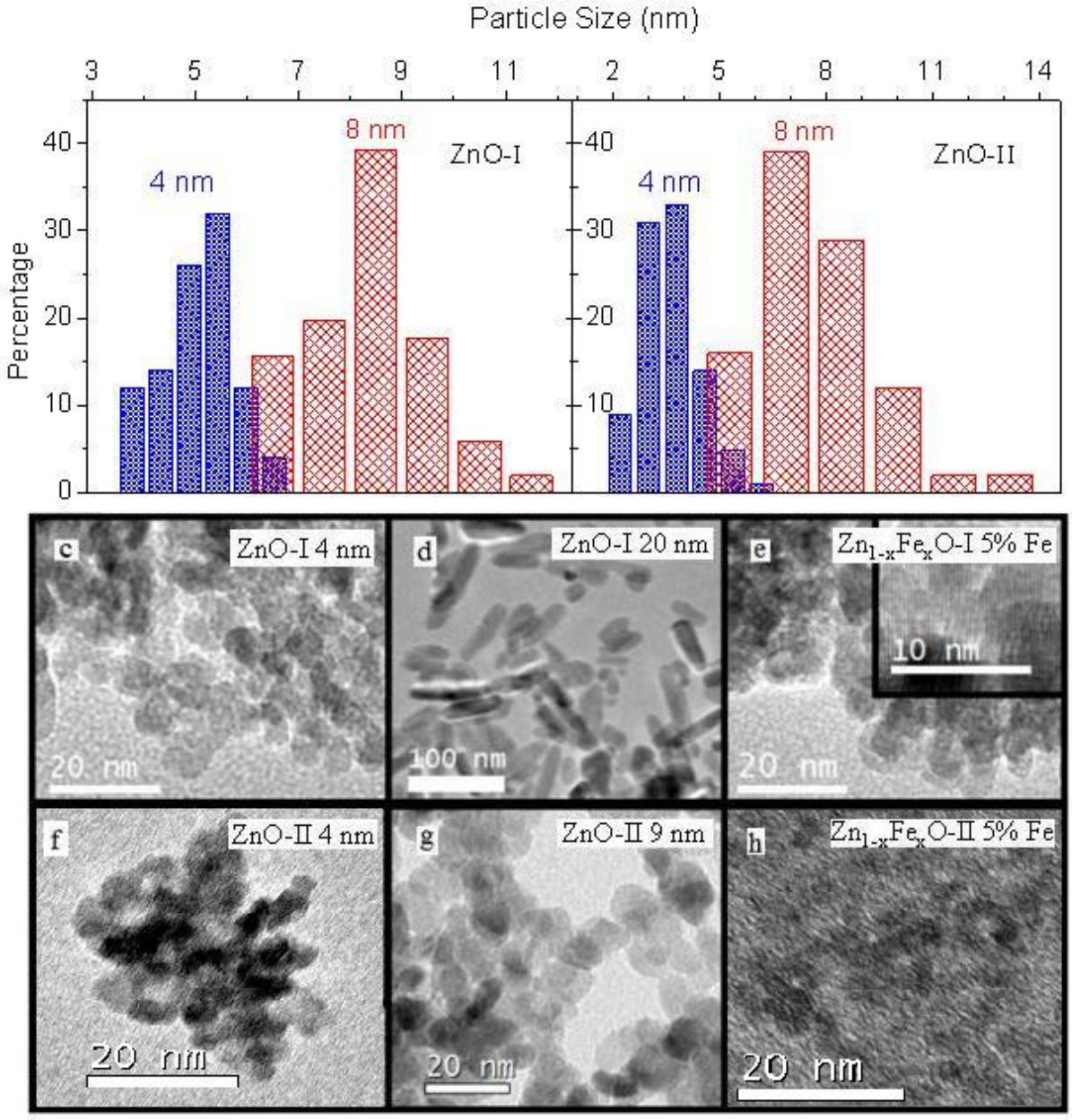

Figure 2, L. Johnson et al (color online, double column figure)

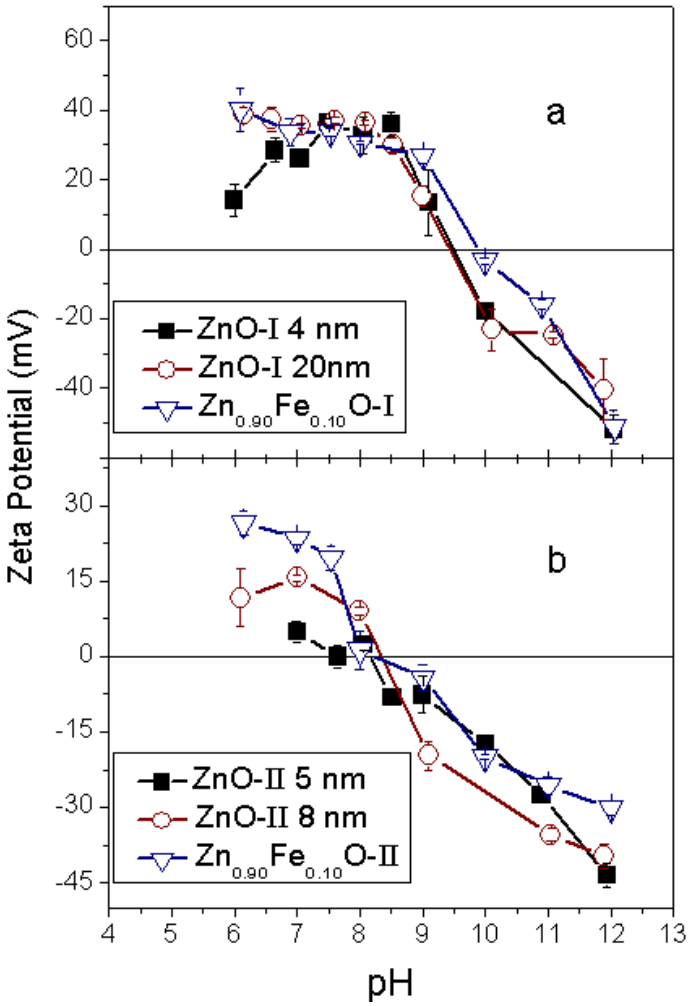

Figure 3, L. Johnson et al (color online)

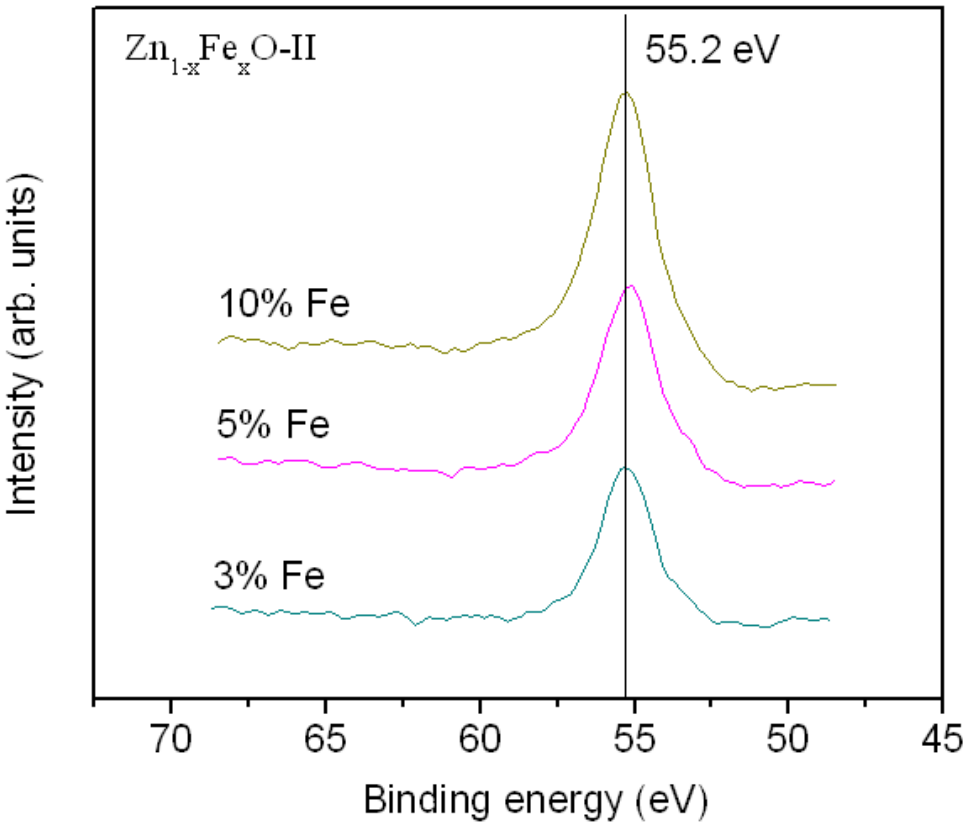

Figure 4, L. Johnson et al (color online)

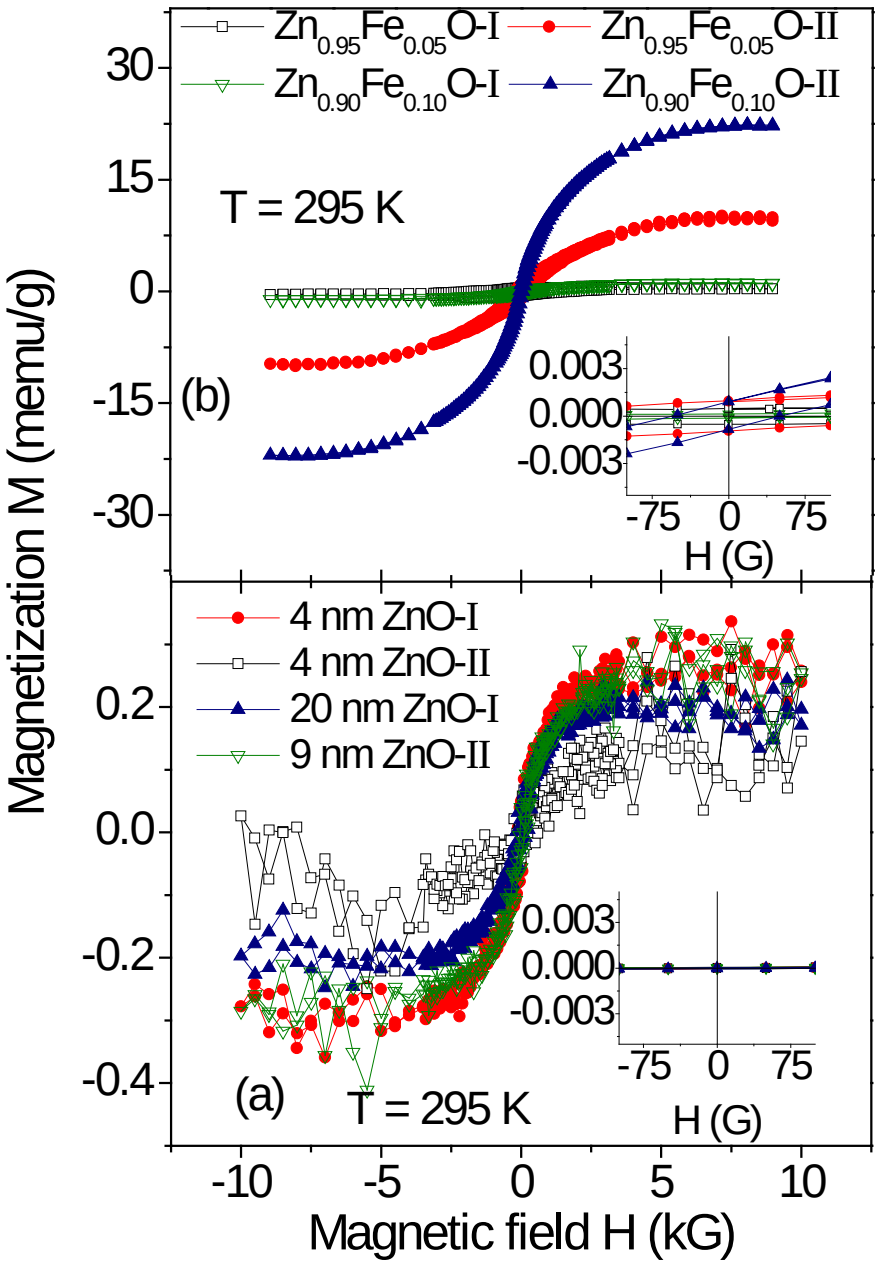

Figure 5, L. Johnson et al (color online)

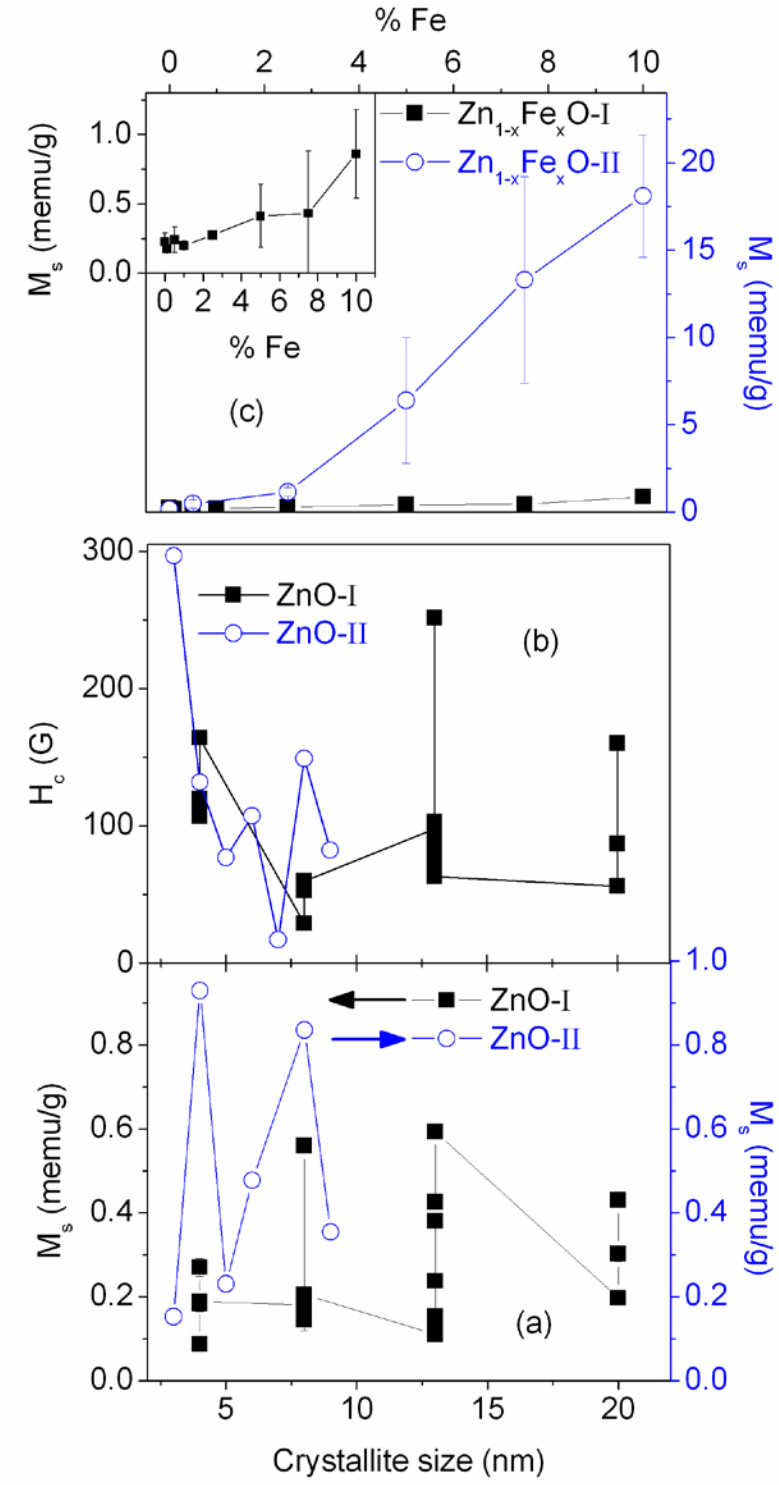

Figure 6, L. Johnson et al (color online)

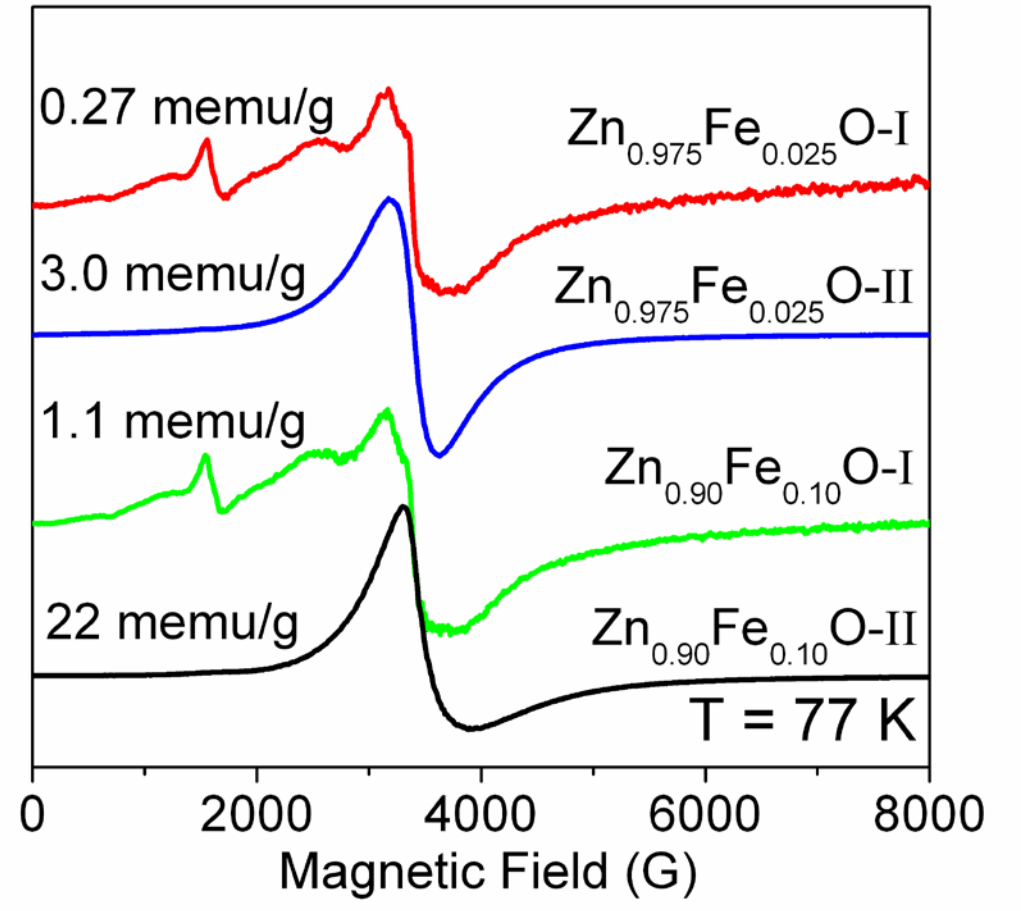

Figure 7, L. Johnson et al (color online)

References

1. T. Dietl, A. Haury, and Y.M. d'Aubigne, Physical Review B. **55** R3347 (1997).
2. K. Sato and H. Katayama-Yoshida, Physica B-Condensed Matter. **308** 904 (2001).
3. T. Dietl, H. Ohno, F. Matsukura, J. Cibert, and D. Ferrand, Science. **287** 1019 (2000).
4. A. Sundaresan, R. Bhargavi, N. Rangrajan, U. Siddesh, and C.N.R. Rao, Physical Review B. **74** 161306 (2006).
5. D. Gao, Z. Zhang, J. Fu, Y. Xu, J. Qi, and D. Xue, Journal of Applied Physics. **105** 113928 (2009).
6. M.A. Garcia, J. M. Merino, E. Fernndez Pinel, A. Quesada, J. de la Venta, M. L. Ruíz Gonzlez, G. R. Castro, P. Crespo, J. Llopis, J. M. Gonzlez-Calbet, and A. Hernando Nano Letters. **7** 1489 (2007).
7. S. Kumar, Y.J. Kim, B.H. Koo, S. Gautam, K.H. Chae, R. Kumar, and C.G. Lee, Materials Letters. **63** 194 (2009).
8. J.M.D. Coey, M. Venkatesan, P. Stamenov, C.B. Fitzgerald, and L.S. Dorneles, Physical Review B. **72** 024450 (2005).
9. H.H. Hong, I. Sakai, N. Poirot, and V. Brize, Physical Review B. **73** 132404 (2006).
10. S.D. Yoon, Y. Chen, A. Yang, T.L. Goodrich, X. Zuo, K. Ziemer, C. Vittoria, and V.G. Harris, Journal of Magnetism and Magnetic Materials. **309** 171 (2007).
11. V. Fernandes, R.J.O. Mossanek, P. Schio, J.J. Klein, A.J.A. de Oliveira, W.A. Ortiz, N. Mattoso, J. Varalda, W.H. Schreiner, M. Abbate, and D.H. Mosca, Physical Review B. **80** 035202 (2009).
12. P. Esquinazi, D. Spemann, R. Hohne, A. Setzer, K.H. Khan, and T. Bultz, Phys. Rev. Lett. **91** 227201 (2003).
13. G. Kopnov, Z. Vager, and R. Naaman, Advanced Materials. **19** 925 (2007).
14. P. Crespo, R. Litrán, T. C. Rojas, M. Multigner, J. M. de la Fuente, J. C. Sánchez-López, M. A. García, A. Hernando, S. Penadés, and A. Fernández, Physical Review Letters. **93** 087204 (2004).
15. I. Carmeli, G. Leitus, R. Naaman, S. Reich, and Z. Veger, Journal of Chemical Physics. **118** 10372 (2003).
16. K.M. Reddy, K. Feris, J. Bell, D. G. Wingett, C. Hanley, and A. Punnoose, Applied Physics Letters. **90** 213902 (2007).
17. J. Hays, K. M. Reddy, N. Graces, M. H. Engelhard, V. Shutthanandan, N. Giles, C. Wang, S. Thevuthasan and A. Punnoose,, Journal of Physics: Condensed Matter. **19** 266203 (2007).
18. J. Hays, A. Punnoose, R. Baldner, M.H. Engelhard, J. Peloquin, and K.M. Reddy, Physical Review B. **72** 075203 (2005).
19. A. Punnoose, H. Magnone, M.S. Seehra, and J. Bonevich, Physical Review B. **64** 174420 (2001).
20. N.S. McIntyre and D.G. Zetaruk, Analytical Chemistry. **49** 1521 (1977).
21. A. Punnoose, J. Hays, A. Thurber, M.H. Engelhard, R.K. Kukkadapu, C. Wang, V. Shutthanandan, and S. Thevuthasan, Physical Review B. **72** 054402 (2005).
22. W.M. Walsh Jr., L.P. Rupp Jr., Physical Review **126** 952 (1962).
23. D.V. Azamat and M. Fanciulli, Physica B. **401-402** 382 (2007).

24. L. Ju-Fen, K. Xiao-Yu, M. Ai-Jie, and T. Xiao-Ming, Chemical Physics Letters. **429** 266 (2006).
25. J.M.D. Coey, M. Venkatesan, and C.B. Fitzgerald, Nature Materials. **4** 173 (2005).
26. J.M.D. Coey, K. Wongsaprom, J. Alaria, and M. Venkatesan, Journal of Physics D: Applied Physics. **41** 134012 (2008).